Efficient Raman sideband cooling of trapped ions to their motional ground state

H. Che, K. Deng,* Z. T. Xu, W. H. Yuan, J. Zhang, and Z. H. Lu†

MOE Key Laboratory of Fundamental Physical Quantities Measurements, Hubei Key Laboratory of Gravitation and Quantum Physics, School of Physics, Huazhong University of Science and Technology, Wuhan 430074, People's Republic of China

(Received 28 April 2017; published 17 July 2017)

Efficient cooling of trapped ions is a prerequisite for various applications of the ions in precision spectroscopy, quantum information, and coherence control. Raman sideband cooling is an effective method to cool the ions to their motional ground state. We investigate both numerically and experimentally the optimization of Raman sideband cooling strategies and propose an efficient one, which can simplify the experimental setup as well as reduce the number of cooling pulses. Several cooling schemes are tested and compared through numerical simulations. The simulation result shows that the fixed-width pulses and varied-width pulses have almost the same efficiency for both the first-order and the second-order Raman sideband cooling. The optimized strategy is verified experimentally. A single $^{25}Mg^{+}$ ion is trapped in a linear Paul trap and Raman sideband cooled, and the achieved average vibrational quantum numbers under different cooling strategies are evaluated. A good agreement between the experimental result and the simulation result is obtained.

DOI: 10.1103/PhysRevA.96.013417

I. INTRODUCTION

Since cold trapped ions are well isolated from the environment, they are widely used in different fields such as precision spectroscopy [1–5], quantum simulation [6,7], and quantum information processing [8,9]. The motion of a trapped ion can be described as a simple harmonic oscillation and its motional state can be expressed as motional eigenstates $|n\rangle$. For implementing quantum logic [10] and quantum computation [11], many schemes require the motional states of the ion to be cooled to the ground state ($n = 0$). Raman sideband cooling and optical sideband cooling [12] are two effective methods to cool ions such as Be^{+} [13], Mg^{+} [14–16], Cd^{+} [17], and Ca^{+} [18] to their motional ground state.

There are two important aspects to be considered for motional ground-state cooling. The first is the lowest achievable mean quantum number of motional states $\overline{n}$. As this number becomes smaller, the probability that the ions are in the motional ground state becomes larger. In this case, quantum gate protocols and quantum-logic-spectroscopy protocols can be easily implemented and decoherence effects from residual thermal motion can be minimized. The second is the time spent on cooling. The time shall be as short as possible, so that we can decrease the total quantum logic gate operation time. This issue is especially important in ion optical clocks. A fast cooling rate means a short dark time in the operation of an optical clock, and the dark time limits the stability of the clock due to the Dick effect [19]. Here we will concentrate on how to implement Raman sideband cooling on ions with a simple and efficient strategy.

Raman sideband cooling often starts with a Doppler cooled ion, which has a $\overline{n}$ ranging from 10 to 100 depending on the Doppler cooling result. After that, a series of sideband cooling and repumping pulses are applied to reduce the $\overline{n}$ to near zero. If the ion is in a Fock state $|n\rangle$, the cooling strategy may be simple. The cooling sequence can be composed by a series of π pulses with pulse times of $\tau_{n,n-1}$, $\tau_{n-1,n-2}$, ..., where $\tau_{n,n-1}$ is the π-pulse time for the Fock state $|n\rangle$ and $\tau_{n-1,n-2}$ is the π-pulse time for the Fock state $|n-1\rangle$, etc. However, in reality the ion's initial motional state $|n\rangle$ is thermally distributed; therefore, one shall consider the contributions of over 100 different motional states. Different motional states require different Rabi frequencies and π-pulse times. During the cooling process, the motional state distribution will change and the cooling strategy becomes more complicated. The pulse times can be chosen to be fixed or varied in the cooling process. For the varied-width scheme, the last Raman pulse time is set to correspond to a π-pulse time from the $n = 1$ state to the $n = 0$ state while the durations of the earlier pulses are set shorter [13]. For the fixed-width scheme, a constant π-pulse time is set for the whole Raman sideband cooling process. Both of the two schemes have been used before, but the exact difference between these two schemes is not clear and has never been discussed in detail before. The fixed-width scheme has been shown to be sufficient for certain experiments [17,20], but whether it can satisfy the stringent requirements of quantum-logic-based optical clocks is still an open question.

In a typical Raman sideband cooling process, according to the initial average $\overline{n}$ and Lamb-Dicke parameter, either the first-order or the second-order red sideband (RSB) Raman pulses can be used. Here the first-order and the second-order RSB Raman pulses reduce the vibration phonon by one and two. Normally the second-order RSB Raman pulses are more efficient than first-order RSB Raman pulses in cooling higher n states. However, since they cannot be used to cool the motional state of $n = 1$ any further, when the $\overline{n}$ of the ion becomes smaller and a larger population accumulates at the $n = 1$ state, the second-order RSB Raman pulses will not work. Furthermore, there exist certain Fock states $|n\rangle$ for which the Rabi frequencies of the first-order RSB Raman pulses or the second-order RSB Raman pulses equal to zero. Therefore, the second-order RSB Raman pulses and the first-order RSB Raman pulses are often used together in order to cool the ion to the motional ground state [14]. How to arrange the pulse sequences of them is an important issue to be considered in order to realize efficient cooling.

*ke.deng@hust.edu.cn
†zehuanglu@hust.edu.cn

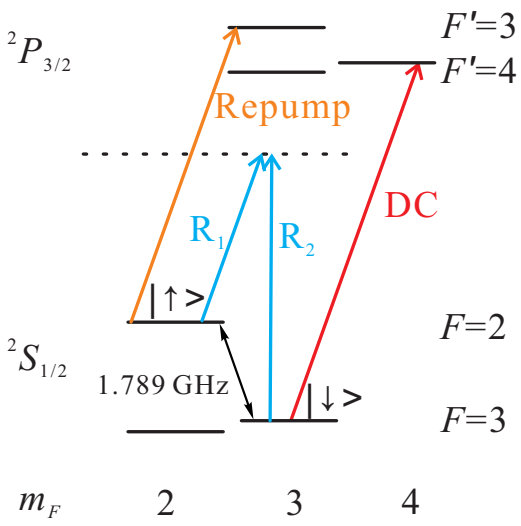

FIG. 1. The relevant energy levels of $^{25}Mg^+$ and laser beams used. R_1 and R_2, Raman beams; DC, Doppler cooling beam; and Repump, repumping beam. $|\downarrow\rangle = {}^2S_{1/2}|3,3\rangle$, $|\uparrow\rangle = {}^2S_{1/2}|2,2\rangle$.

In this paper we report the simulation on the Raman sideband cooling process with different cooling strategies. The average $\overline{n}$ of the ion during the cooling process is calculated. The situations under different pulse times for both second-order RSB Raman pulses and first-order RSB Raman pulses are compared. The fixed-width pulse sequence and the varied-width pulse sequence are also compared. How to best combine the second-order RSB Raman pulses and first-order RSB Raman pulses is analyzed. Based on the simulation results, the best cooling strategy is suggested. Then we perform an experiment to verify the simulation results. We trapped a single $^{25}Mg^+$ ion in a linear Paul trap and implement Raman sideband cooling with different cooling strategies. The achievable average $\overline{n}$ of the ion under different cooling strategies are measured and compared. The experimental results agree well with our simulation results.

II. BASIC THEORY

Figure 1 shows the relevant energy levels of $^{25}Mg^+$ ions and can be used to illustrate the principle of Raman sideband cooling implemented in our experiment. In the beginning, the ion is Dopper cooled and optically pumped into the $|\downarrow\rangle = {}^2S_{1/2}|F = 3, m_F = 3\rangle$ state (in the following, it will be written as ${}^2S_{1/2}|3,3\rangle$ for simplicity) through a closed cycling transition from $|\downarrow\rangle$ to ${}^2P_{3/2}|4,4\rangle$. Raman sideband cooling is implemented with the Doppler-cooled single trapped $^{25}Mg^+$ ion. Typically the initial average motional level $\overline{n}$ can be from 10 to 100, depending on the Doppler cooling temperature. RSB π pulses are used to reduce the number $\overline{n}$. The π-pulse time is decided by the Rabi frequency of Raman transition between $|\downarrow\rangle|n\rangle$ and $|\uparrow\rangle|n'\rangle$,

$$\tau_{n',n} = \pi/\Omega_{n',n}, \tag{1}$$

where the Rabi frequency is given by [21]

$$\Omega_{n',n} = \Omega_0 e^{-\eta^2/2}\sqrt{\frac{n_<!}{n_>!}}\eta^{|n'-n|}L_{n_<}^{|n'-n|}(\eta^2). \tag{2}$$

Here Ω_0 is the Rabi frequency of the atomic transition, not taking into account the motional state contributions. $n_<(n_>)$ is the smaller (larger) of n' and n, η is the Lamb-Dicke parameter, and L is the generalized Laguerre polynomial,

$$L_n^\alpha(X) = \sum_{m=0}^{n}(-1)^m\binom{n+\alpha}{n-m}\frac{X^m}{m!}. \tag{3}$$

For $n = n' = 0$, we have $\Omega_{0,0} = \Omega_0\exp(-\eta^2/2)$. The exponential reduction of the Rabi frequency is due to contribution of other motional states. These states reduce the Rabi frequency in much the same way as lattice vibrations affect a single emitter or scatter embedded in a crystal, as described by the Debye-Waller effect [22].

With proper RSB π pulses applied, the ion is transferred to the $|\uparrow\rangle$ state and the motional quantum number is reduced from n to n'. Then the ion needs to be repumped to $|\downarrow\rangle$ while keeping the motional number n' the same. This sequence is repeated to reduce the $\overline{n}$ to near zero.

For ions in the trap, based on thermal distribution each motional state population probability is given by

$$P_n = \frac{\overline{n}}{(\overline{n}+1)^{n+1}}. \tag{4}$$

When a pulse is applied, the state population will change. For example, when a first-order RSB pulse is applied, the state of $|n\rangle$ is changed to $|n-1\rangle$ with probability $P_{n\to n-1}$, and the state of $|n+1\rangle$ is changed to $|n\rangle$ with probability $P_{n+1\to n}$; therefore, the population probability P_n will become $P_n + P_{n+1}P_{n+1\to n} - P_nP_{n\to n-1}$, where the transition probability $P_{n\to n-1}$ is given by

$$P_{n\to n-1} = \sin^2\left(\frac{\Omega_{n,n-1}t}{2}\right). \tag{5}$$

The updated $\overline{n}$ can then be obtained from the values of P_n. After repumping and applying a second RSB cooling pulse, the population of each motional state will change according to the same principle and a new $\overline{n}$ will be produced. Based on the above theory, the evolution of the $\overline{n}$ in the cooling process can be obtained.

Here the decoherence effect [23] due to thermal fluctuations caused by laser repumping is neglected for simplicity. For a Raman-sideband-cooled ion, the repumping laser will heat the ion and increase the phonon number by [24]

$$\Delta\overline{n} = \frac{ts_{re}\Gamma_{re}^3\eta^2}{4\Delta_{HF}^2}. \tag{6}$$

Here t is the time of laser repumping, s_{re} is the saturation parameter of the repumping laser, and Γ_{re} is the natural linewidth of the repumping transition. For $^{25}Mg^+$ ions, $\Delta_{HF} = 2\pi \times 1.789$ GHz corresponds to the hyperfine splitting of the ground state, and Γ_{re} is $2\pi \times 41.3$ MHz. For $s_{re} = 1$ and $\eta = 0.3$, the heating effect by the 10-μs repumping laser is about $\Delta\overline{n} = 0.03$. Therefore, the probability of increasing n during repumping can be neglected when $\overline{n} > 1$. Only when $\overline{n}$

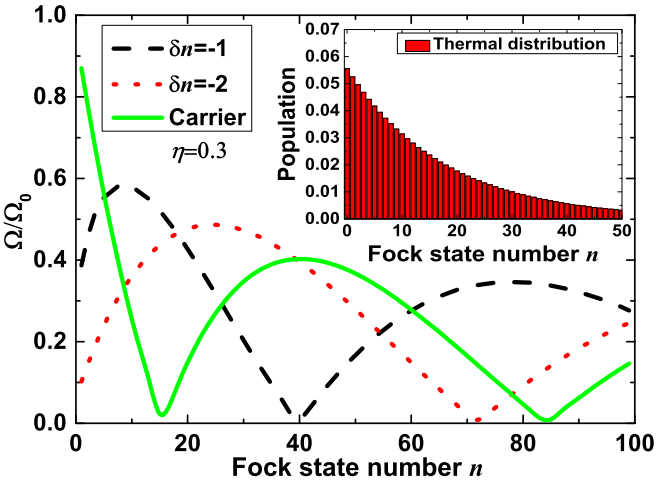

FIG. 2. The relative Rabi frequencies of carrier transitions (solid green line), first-order RSB transitions (dashed black line), and second-order RSB transitions (dotted red line) as a function of Fock state number n. The inset shows the theoretical population of a thermal distribution for $\overline{n} = 17$.

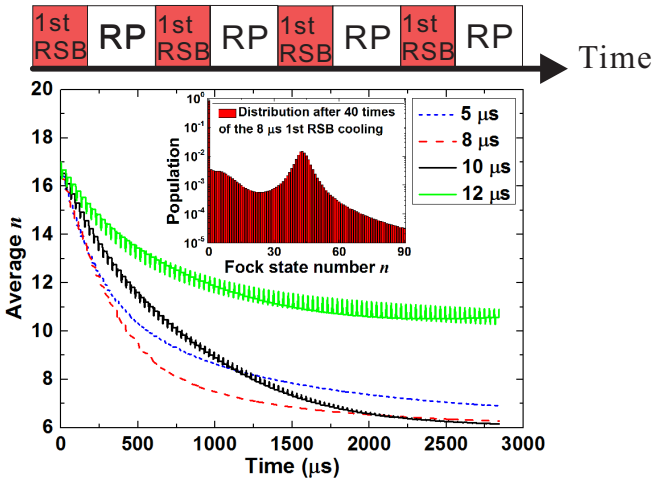

FIG. 3. Simulated average n as a function of time with the first-order RSB cooling for 5 μs (short dashed blue line), 8 μs (long dashed red line), 10 μs (solid black line), and 12 μs (solid green [light gray] line). The inset shows the simulated population distribution after 40 times of the 8-μs first-order RSB cooling. The top shows a scheme of the pulse sequence in the figure. RP, repumping pulses.

is cooled to far less than 1 does the heating effect of the laser repumping become important.

III. SIMULATION RESULT

We assume the initial average motional phonon number is 17, which is chosen according to the Doppler cooling result in our experiment. The initial average motional number $\overline{n}$ of the Doppler-cooled ion can be obtained through the ratio of the excitation probabilities of the rth order RSB and BSB by [25]

$$Q = \frac{\rho_r^{\mathrm{RSB}}(t)}{\rho_r^{\mathrm{BSB}}(t)} = \left(\frac{\overline{n}}{1+\overline{n}}\right)^r. \tag{7}$$

Due to the thermal distribution, the distribution of the motional states covers from 0 to more than several hundreds. The inset of Fig. 2 depicts a thermal distribution with an average $\overline{n}$ of 17. In the simulation, we consider 151 motional states (from 0 to 150). They take up 99.99% of the all population. For each Fock state, the Raman pulse interacts with the ion and changes its motional quantum state with certain probability. The population will have a new distribution. After that, the ion is repumped and we assume the distribution is the same for simplicity. As described above, the heating by a 10-μs repumping laser is about $\Delta\overline{n} = 0.03$. So we assume the distribution remains the same after repumping when $\overline{n} > 1$. Subsequently, the second cooling pulse is applied, and each Fock state interacts with it with a new population distribution. The process will be repeated many times until we reach the motional ground state.

In a typical Raman sideband cooling process, the applied RSB Raman pulses can be either first-order RSB Raman pulses or second-order RSB Raman pulses, which will reduce the quantum phonon number by one or two, respectively. Considering the heating effect of 10-μs laser repumping, the largest theoretical possible cooling rates are 0.97 and 1.97 phonons per cooling cycle for the first-order and second-order RSB cooling, respectively. Here a cooling cycle is composed of a cooling pulse and corresponding repumping pulses.

Figure 2 shows the Rabi frequencies of carrier transitions, first-order RSB transitions, and second-order RSB transitions as a function of Fock state number n. It can be seen that different Fock states have different Rabi frequencies, and therefore they have different π-pulse times. We have to choose a proper initial pulse time. Many Raman sideband cooling pulses will be needed to reduce the $\overline{n}$ to near zero. During the cooling process, the population distribution will change and become more complicated. Simulations are performed to determine which sequence is better. It shall be noted that the Rabi frequencies are almost zero for certain Fock states according to Fig. 2. Therefore, how to arrange the combination of first-order RSB pulses and second-order RSB pulses is also an important issue to be considered.

First, we consider the cooling sequence with the fixed-width cooling pulses. In the simulation, we take an average Rabi frequency $\Omega_0/2\pi$ as 150 kHz and η as 0.3. For the pulse time, we use four representative times: 5, 8, 10, and 12 μs in the simulation. Figure 3 shows the evolution of the average motional phonon number $\overline{n}$ as a function of the cooling time for the first-order RSB Raman pulse cooling. The repumping time is set to be 20μs (including laser repumping and RF repumping). From the results in Fig. 3, we can see that different pulse times have different cooling efficiency. The 8-μs pulses are the most efficient pulses. It means that 8-μs pulses are the most likely π pulses for the ion during the cooling process. From the figure, it can be seen that for a proper chosen pulse time the $\overline{n}$ decreases rapidly, while for an unsuitable pulse time the $\overline{n}$ decreases much more slowly. The first 8-μs cooling pulse reduces the phonon number n by about 0.65, which is about 2/3 of the largest theoretical cooling rate. After that, the cooling rate decreases. The reason is that part of the population accumulates at $|n\rangle = 0$, which cannot be further cooled, and part of the population accumulates at $|n\rangle$ whose

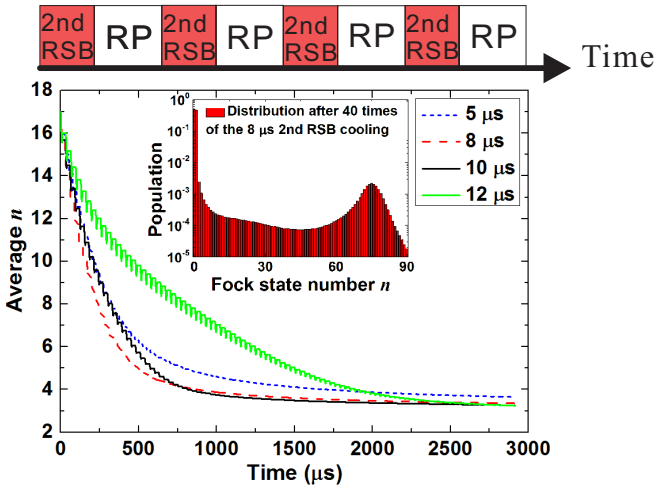

FIG. 4. Simulated average n as a function of time with the second-order RSB cooling for 5 μs (short dashed blue line), 8 μs (long dashed red line), 10 μs (solid black line), and 12 μs (solid green [light gray] line). The inset shows the simulated population distribution after 40 times of the 8-μs second-order RSB cooling. The top shows a scheme of the pulse sequence in the figure. RP, repumping pulses.

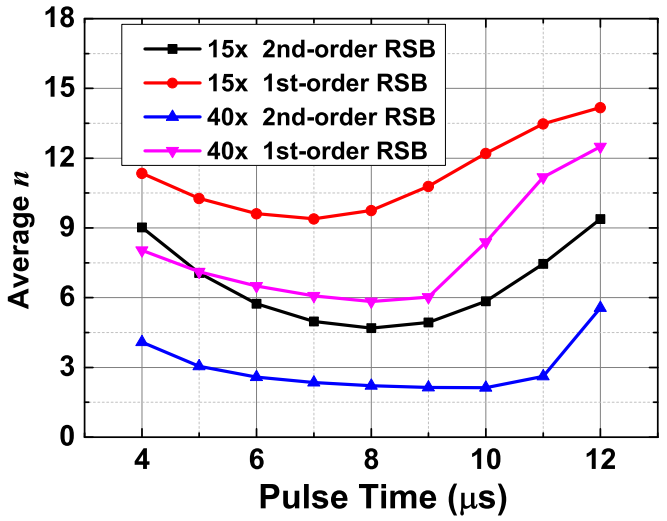

FIG. 5. Simulated average population as a function of the pulse time for the 1st-order RSB cooling and the 2nd-order RSB cooling. The numbers of cooling pulse for them are chosen to be 15 and 40.

Rabi frequency is near zero. The inset of Fig. 3 shows the population distribution after 40 times of the 8-μs first-order RSB cooling. It can be seen that part of the population accumulates around $|n\rangle = 43$. We also simulate for more cooling cycles. The results show that the accumulation center is $|n\rangle = 41$ for 150 cooling cycles and $|n\rangle = 40$ for 500 cooling cycles. According to Fig. 2, the zero crossing of the first-order RSB Rabi frequency is at $|n\rangle = 40$. Therefore, for longer times the population decay curves in Fig. 3 approach asymptotic values that are larger than 0.

For the second-order RSB Raman cooling, different pulse times from 5 to 12 μs are also compared, as shown in Fig. 4. The first 8-μs cooling pulse reduces the phonon number n by about 1.5, which is about 3/4 of the largest theoretical cooling rate. Then the cooling rate decreases for the same reason as mentioned above. The inset of Fig. 4 shows the population distribution after 40 times of the 8-μs second-order RSB cooling. It can be seen that part of the population accumulates at $|n\rangle = 75$. We also simulate for more cooling cycles. The results show that the accumulation center is $|n\rangle = 73$ for 150 cooling cycles and $|n\rangle = 72$ for 500 cooling cycles. According to Fig. 2, the zero crossing of the second-order RSB Rabi frequency is at $|n\rangle = 72$. Therefore, for longer times the population decay curves in Fig. 4 also have asymptotic values that are larger than 0. Figure 5 shows the average population as a function of the pulse time for both the first-order RSB cooling and the second-order RSB cooling. The numbers of cooling pulse for them are chosen to be 15 and 40. Number 15 corresponds to the optimum switch point in a second-order RSB cooling and first-order RSB cooling combination scheme that will be discussed later in the paper. From the figure it can be seen that when the pulse time is chosen to be around 8 μs the cooling scheme is quite robust. When the laser power has a 10% fluctuation, which means that the Rabi frequency has a 5% variation, the cooling results only change about 1.5%.

Next we compare the fixed-width pulses sequence and varied-width pulses sequence. The fixed-width pulses all have pulse width of 8 μs, which are the most efficient pulses in cooling according to the results in Figs. 3 and 4. For the varied-width pulses, each pulse time is changed according to the corresponding Rabi frequency of different motional level n. For the second-order RSB Raman cooling, the pulse times are set to be $\tau_{18,16}$, $\tau_{17,15}$, $\tau_{16,14}$, and so on according to Eq. (2). The last pulse time is $\tau_{2,0}$. For the first-order RSB Raman cooling, the pulse times are set to be $\tau_{17,16}$, $\tau_{16,15}$, and so on, and the last one is $\tau_{1,0}$. The results of four different situations are shown in Fig. 6. The starting motional levels for all four situations are the same, which is $n = 17$. From the figure we can see that the fixed-width pulses and varied-width pulses have almost the same efficiency for both the first-order RSB and the second-order RSB cooling. From Fig. 2, the Rabi frequency for each $|n\rangle$ is quite different. Therefore, any π pulse is only suitable for part of the total population, whether the π pulse is fixed width or varied width. From Fig. 6, we can see that the second-order RSB pulses are more efficient at the beginning of cooling. But the cooling rate becomes smaller, and after 400 μs the second-order RSB pulses cannot cool the ion anymore. At this stage the $\bar{n}$ is still as large as 4. Therefore, the first-order RSB pulses are also needed at the later stage according to our previous analysis. A proper combination of them should be explored, and we perform further simulation to find the best switch point.

In the simulation, we compare different switch points from the second-order RSB cooling to the first-order RSB cooling. From the result, it shows that the optimum switch point is after application of 15 to 20 second-order RSB pulses. We choose the 15-pulse-point as the switch point and start applying the first-order RSB cooling. After the application of these first-order RSB pulses, the $\bar{n}$ can decrease quickly and ultimately it is reduced to about 2. However, after 15 first-order RSB cooling pulses, the cooling rate becomes small again. To further cool the ion, another 15 second-order RSB pulses and 30 first-order RSB pulses are followed. In the simulation the

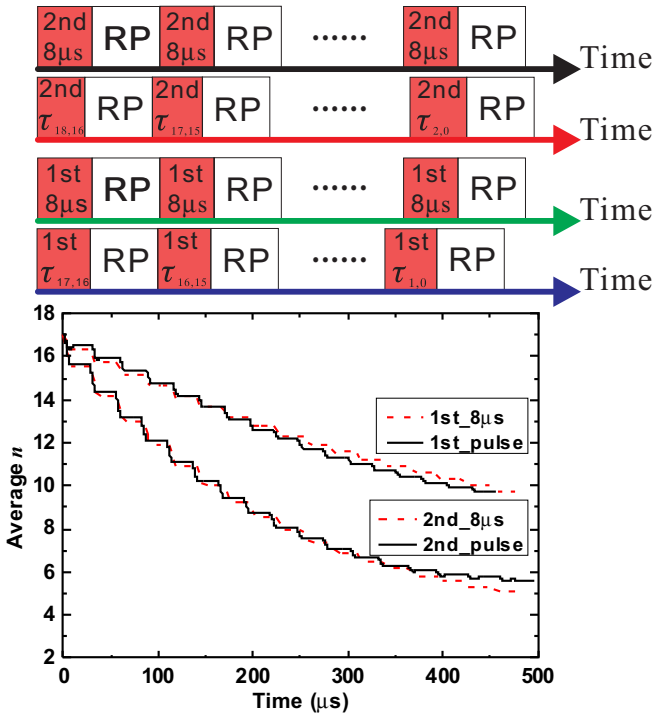

FIG. 6. Simulated average n as a function of time with the second-order RSB cooling (lower lines) and the first-order RSB cooling (upper lines) with fixed-width (dashed red lines) and varied-width (solid black lines) pulses. The top shows a scheme of the pulse sequence in the figure.

decoherence effect is considered [23] and the coherence decay rate is set to be 500 Hz. All the fixed-width pulses are set to be 9 μs. The result is shown in Fig. 7. The ion is cooled to $\overline{n} < 0.05$. Considering the effect of Raman scattering, the limit of Raman sideband cooling is [26]

$$\langle \overline{n} \rangle_{min} = C_S(\gamma/\omega_z)^2. \tag{8}$$

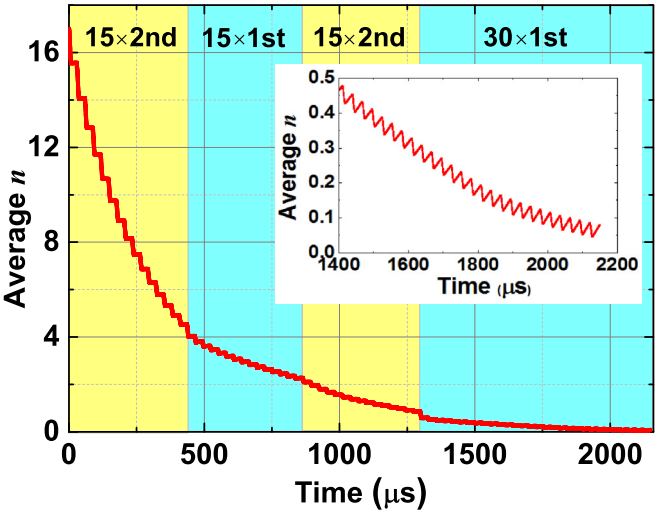

FIG. 7. Simulated average n as a function of time with a combination of the 2nd-order RSB cooling and the 1st-order RSB cooling. Inset shows the detail of the curve after 1400 μs.

Here γ is the linewidth of the Raman transition, ω_z is the secular motion frequency along the trap axis, and C_S is a constant on the order of 1. For a typical ω_z of 1.5 MHz and γ of less than 1 kHz, the cooling limit is less than 5×10^{-7}. For typical experimental conditions, the linewidth of the Raman transition is broadened due to the Raman laser's linewidth and external magnetic field fluctuation. If γ is broadened to 0.1 MHz, the limit will be 0.004. However, the repumping laser can introduce heating effect. For $^{25}Mg^+$ ions, if the saturation parameter of the repumping laser is 1 and Lamb-Dicke parameter is 0.3, it will lead to a minimum $\overline{n}$ of 0.03 for a typical repumping time of 10 μs [24]. For both fixed-width and varied-width schemes, they have the same cooling limit, which depends on the heating effect of the repumping process. Therefore, the above cooling sequence is suitable for the motional ground-state cooling. We also simulate with slightly different pulse times in the ± 0.2-μs range and the results are almost the same. From all the simulation results we can conclude that the fixed-width pulse sequence is efficient enough in Raman sideband cooling. Since the fixed-width pulses strategy is easier to be implemented in practice, it will be adopted in our experiment. Moreover, through proper alternate applications of the second-order RSB pulses and the first-order RSB pulses in the cooling sequence, higher cooling efficiency can be achieved.

IV. EXPERIMENTAL RESULT

To verify the simulation results, we trap a single $^{25}Mg^+$ ion in a linear Paul trap [27,28] and implement Raman sideband cooling with different cooling strategies. The linear trap consists of four blade-shaped electrodes and two end-cap tip electrodes. Two opposing blade-shaped electrodes are fed with a high-voltage RF power and the other two are grounded. The distance between the two opposing blade-shaped electrodes is $2r = 1.6$ mm. These four blade electrodes supply the radial confinement for ions. The distance between the two end-cap electrodes is $2z = 4.0$ mm. dc voltages are applied to the end-cap electrodes. These two end-cap electrodes supply the axial confinement for ions. The secular motion frequency along the trap axis is typically 1.5 MHz with 300-V end-cap voltage. Three external rods running along the trap axis direction are used for the compensation of stray electric fields in radial directions. The axial compensation is implemented on the end-cap electrodes.

To drive the trap, a high-voltage RF power supply is needed. The high-voltage RF power supply with a frequency of 23.76 MHz is first produced by a frequency synthesizer and an RF amplifier. Then a homemade helical resonator [29] with a quality factor of about 300 is used to apply the RF voltage to the trap electrodes. A quarter-wave antenna made with aluminum is put inside the vacuum chamber, connected with the feedthrough of the vacuum chamber. The antenna is designed with a resonance frequency of 1.789 GHz. A Mg oven is installed at the bottom of the vacuum chamber. Two fused silica re-entrant viewports are installed on the vacuum chamber to collect the fluorescence of the ions. Two sets of imaging lens system are installed. One is for a photon-counting module and the other is for an electron-multiplying CCD. The fluorescence collection efficiency is about 0.4%. A 40-L/s ion

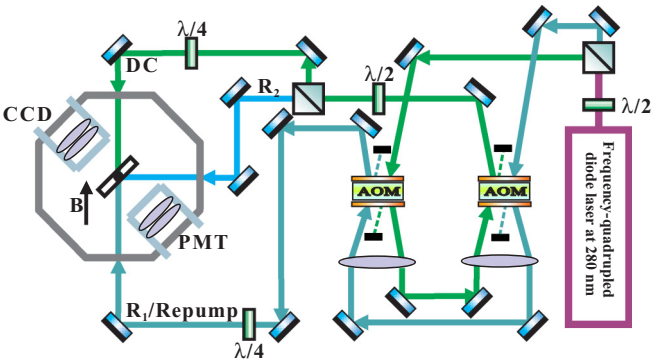

FIG. 8. Schematic of the experimental setup. R_1 and R_2 are the two Raman laser beams as shown in Fig. 1. DC, Doppler cooling laser; Repump, the repumping laser; $\lambda/2$, half wave plate; $\lambda/4$, quarter wave plate. The magnetic field is aligned with the R_1 laser beam. The DC laser beam counterpropagates with the R_1 laser beam.

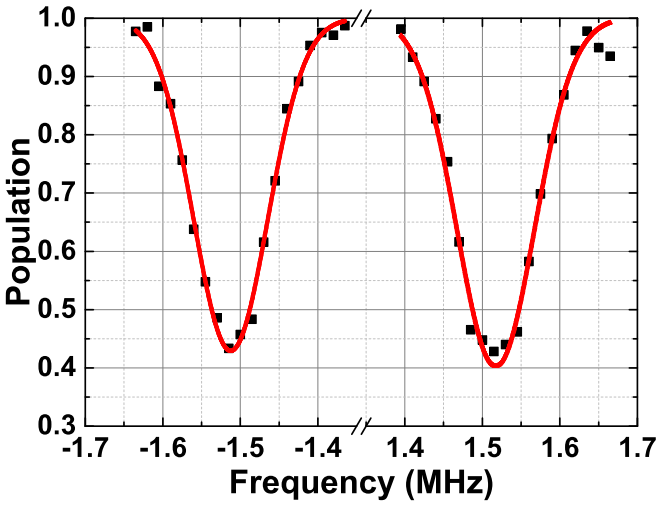

FIG. 9. Raman sideband spectrum of a single $^{25}Mg^+$ ion after Doppler cooling. The average n can be obtained through the BSB-RSB ratio. The calculated value is $\overline{n} = 17(2)$, which is the initial average motional level for the Raman sideband cooling.

pump and a titanium sublimation pump are used to maintain the ultrahigh vacuum environment. The pressure in the vacuum chamber is about 1×10^{-8} Pa.

We use two-photon ionization to create $^{25}Mg^+$ ions from Mg atoms that evaporate out from the Mg oven. The ionization laser is a frequency-quadrupled 285-nm tunable diode laser system. The output power of the laser at 285 nm is 2 mW and the linewidth of the laser is about 2 MHz. A frequency-quadrupled 280-nm laser is used to cool and detect the Mg ions [30]. An electro-optical modulator (EOM) is placed between the two doubling cavities in the 280-nm laser system to generate 9.2-GHz sidebands on a 560-nm green laser beam [14]. The 280-nm laser is frequency tuned such that one of the sidebands coincides with the $^2S_{1/2}$ to $^2P_{3/2}$ transition of $^{25}Mg^+$, which is used for Doppler cooling. When the EOM is switched off, the optical carrier is employed for driving Raman transitions between two hyperfine ground states, as shown in Fig. 1. For Doppler cooling, the laser beam is detuned by half the line width with respect to the closed cycling transition from $|\downarrow\rangle$ to $^2P_{3/2}|4,4\rangle$. We use a Glan laser polarizer to obtain a linearly polarized beam and then a quarter wave plate to obtain a circularly polarized beam. All beams are focused into the center of the trap region. Three pairs of Helmholtz coils are mounted around the vacuum chamber to compensate for stray magnetic field and supply the quantization axis.

Figure 8 shows the schematic of the optical setup. R_1 and R_2 are the two Raman laser beams as shown in Fig. 1. Here R_1 is the circularly polarized (σ) beam and R_2 is the linearly polarized (π) beam. DC is the Doppler cooling beam and repump is the repumping beam. To implement Raman RSB cooling, the transition frequency between $|\downarrow\rangle$ and $|\uparrow\rangle$ should be known first. This frequency is measured by the RF resonant method [14]. The ion is first initialized in the $|\downarrow\rangle$ state by applying the Doppler cooling and repumping beams for 0.3 ms and then interacts with an RF pulse, which transfers the ion to the $|\uparrow\rangle$ state. After that, state detection is achieved by applying the resonant Doppler cooling beam for 50 μs and counting the number of detected photons. The detection pulse width is restricted since the ion can be off-resonantly pumped from the dark state, thus imitating a bright ion which is initially dark. In our system, we typically detect a mean number of five photons for a bright state and a mean number of one photon for a dark state.

For Raman sideband cooling, since the ion needs to be repumped from $|\uparrow\rangle$ to $|\downarrow\rangle$ after each RSB cooling pulse, a series of repumping laser pulses and RF pulses are needed. The transitions for the repumping laser and the 1.789-GHz repumping RF can be seen in Fig. 1. The repumping laser addresses the transition between $|\uparrow\rangle$ to $^2P_{3/2}|3,2\rangle$, since the repumping laser may pump the ion to $^2S_{1/2}|3,2\rangle$ state. Therefore, an RF transition between $|\uparrow\rangle$ and $^2S_{1/2}|3,2\rangle$ frequency is also needed and its frequency should be measured. To measure this repumping RF frequency, we use a similar method as mentioned in Ref. [14]. The ion is first initialized in the $|\downarrow\rangle$ state by applying the Doppler cooling and repumping laser beams. Then an RF π pulse is applied to transfer it to the $|\uparrow\rangle$ state. After that, another RF pulse corresponding to the $^2S_{1/2}|3,2\rangle - |\uparrow\rangle$ transition is applied and final state detection is achieved by applying the resonant Doppler cooling beam. By scanning the frequency of the second RF, the transition frequency between $^2S_{1/2}|3,2\rangle$ and $|\uparrow\rangle$ can be measured.

Before Raman sideband cooling, the initial average motional number $\overline{n}$ of the Doppler cooled $^{25}Mg^+$ ion is measured. This value can be obtained through the BSB-RSB ratio method [13]. Figure 9 shows the BSB transition and RSB transition of the Raman spectrum. For our system we get $\overline{n} = 17(2)$, which is the initial average motional level for Raman sideband cooling. For Raman sideband cooling, resolved Raman sideband pulses are applied after state preparation. Every sideband cooling pulse is followed by three repumping laser pulses and RF pulses. By scanning the Raman transition frequency, a Raman spectrum after cooling is obtained. When the Raman cooling experiment is implemented, we also use the BSB-RSB ratio method to obtain the average $\overline{n}$ to evaluate the cooling efficiency. Previous simulation results reveal a nonthermal distribution after sideband cooling [31]. However, when it is cooled and most of the population is in the motional

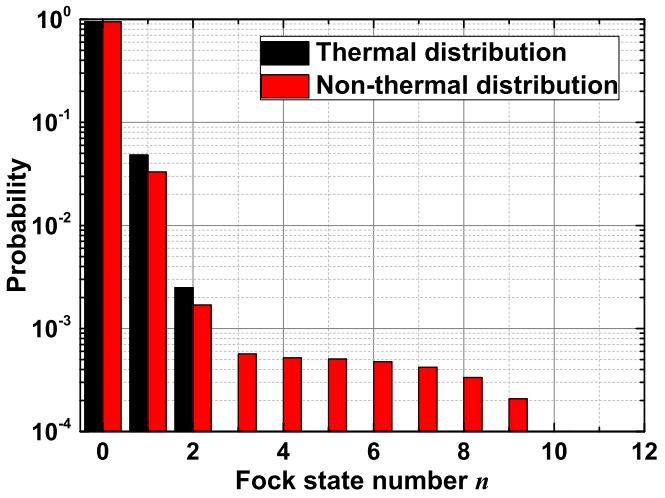

FIG. 10. The thermal distribution and simulated nonthermal distribution for a same average n. The nonthermal distribution is Raman sideband cooled with a cooling scheme as shown in Fig. 7. From the comparison we can see that the ground-state populations are almost the same.

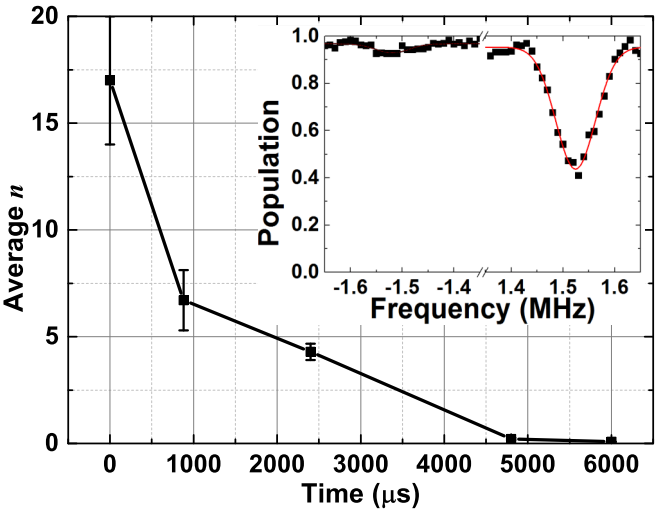

FIG. 12. Measured average n after Raman sideband cooling with optimal cooling strategy. Inset shows the red sideband and blue sideband of Raman spectrum after the Raman sideband cooling process is finished.

ground state, our simulation shows the method is still accurate enough to evaluate the average $\overline{n}$. This situation is of great interest. We simulate a nonthermal distribution and a thermal distribution for a cooled ion; the result is shown in Fig. 10. In the simulation, the decoherence effect due to thermal fluctuations caused by laser repumping is considered [23]. It can be seen that the motional ground-state population ($n = 0$) is almost the same for the two distributions. Therefore, we can use the BSB-RSB ratio method to obtain the average $\overline{n}$ to evaluate the cooling efficiency.

In the experiment, we first cool the ion with only the first-order RSB cooling. Figure 11 shows the average $\overline{n}$ as a function of pulse counts. It can be seen that the curve in Fig. 11 is similar to the curve in Fig. 4 during the cooling process, which shows that the average $\overline{n}$ cannot be continuously reduced after 20 cooling pulses. Then we use the cooling strategy as explained in Fig. 7. In the cooling experiment, each repumping process (including laser and RF repumping) takes 70 μs. The experimental result is shown in Fig. 12 and the ion is ultimately cooled to $\overline{n} = 0.06(4)$. Since the population of $n = 0$ is given by $P(n = 0) = 1 - Q$, the population of $n = 0$ is about 94(4)% after cooling. The total time for cooling is about 6 ms with 90% time used on repumping. Therefore, the total time can be further reduced by increasing the RF power to reduce the RF repumping time.

Heating rate is a factor that can influence multi-ion quantum logic gate fidelities. In addition, for the ion optical clocks, heating rate influences the secular motion time-dilation shift uncertainty [31]. So it is necessary to know the heating rate in the experiment. Based on the Raman sideband detection

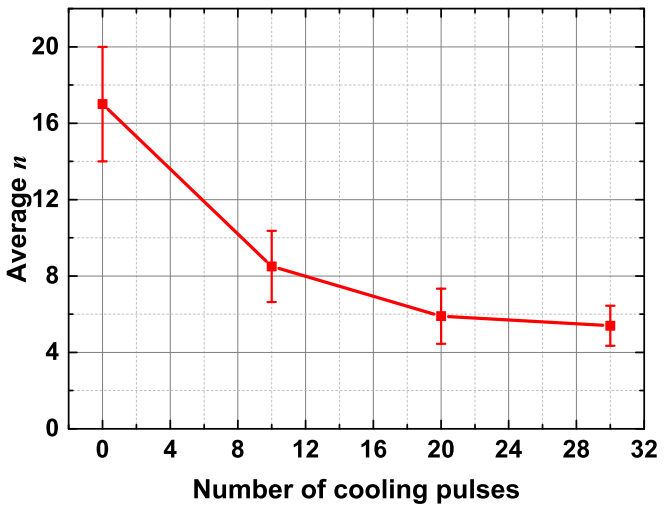

FIG. 11. Measured average n with only the first-order RSB cooling.

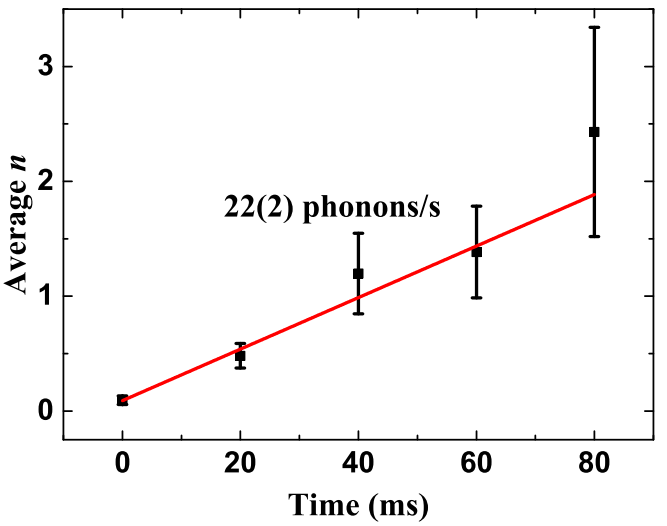

FIG. 13. The average motional quantum number is plotted as a function of the waiting time after motional ground-state cooling. A linear fit yields a heating rate of 22(2) phonons per second.

technique, the heating rate of an ion in the linear Paul trap can be measured [25]. In the experiment, the ion is first cooled to the motional ground state through the Raman sideband cooling, then all the laser beams are switched off for a specific waiting time (typically 0–100 ms). During this time, the ion is subject to environmental perturbations and can be excited to higher motional states. After the waiting time, a Raman analysis pulse is applied and state detection is achieved with the resonant Doppler cooling laser pulse. By scanning the Raman transition frequency, a Raman sideband spectrum is obtained. We use the BSB-RSB ratio method to obtain the average vibrational population number $\overline{n}$. Measuring the $\overline{n}$ as a function of the waiting time yields the heating rate. Figure 13 shows the experimental result on the measurement of heating rate, which is about 22(2) phonons per second. Compared with total average cooling rate of 3 phonons per ms, it is reasonable that we do not need to consider the heating rate in the simulation on the Raman sideband cooling.

V. CONCLUSION

In conclusion, we analyze and simulate the cooling process of Raman sideband cooling with different cooling strategies. Based on our simulation results, we conclude that an efficient cooling strategy consists of fixed-width RSB pulses with alternating the second-order RSB pulses and the first-order RSB pulses. This strategy is easy to implement in the experiment and can reduce the needed cooling pulses efficiently. As a demonstration, we trap a single $^{25}Mg^{+}$ ion in a linear Paul trap and cool it with different cooling sequences. The ion is cooled to motional ground state with a 94(4)% population from $\overline{n} = 17(2)$ in 6 ms with 75 cooling pulses, in comparison with 10- to 15-ms cooling time and 80–120 cooling pulses in Ref. [14]. The experimental results agree well with our simulation results. The idea can be extended to motional ground-state cooling of other ions.

ACKNOWLEDGMENTS

The project is partially supported by the National Basic Research Program of China (Grant No. 2012CB821300), the National Natural Science Foundation of China (Grants No. 11304109, No. 11174095, and No. 91336213), and Program for New Century Excellent Talents by the Ministry of Education.

[1] A. D. Ludlow, M. M. Boyd, J. Ye, E. Peik, and P. O. Schmidt, Rev. Mod. Phys. **87**, 637 (2015).
[2] N. Huntemann, C. Sanner, B. Lipphardt, C. Tamm, and E. Peik, Phys. Rev. Lett. **116**, 063001 (2016).
[3] N. Herschbach, K. Pyka, J. Keller, and T. E. Mehlstäubler, Appl. Phys. B **107**, 891 (2012).
[4] Y. Wan, F. Gebert, J. B. Wübbena, N. Scharnhorst, S. Amairi, I. D. Leroux, B. Hemmerling, N. Lörch, K. Hammerer, and P. O. Schmidt, Nat. Commun. **5**, 3096 (2014).
[5] J. C. J. Koelemeij, B. Roth, A. Wicht, I. Ernsting, and S. Schiller, Phys. Rev. Lett. **98**, 173002 (2007).
[6] R. Blatt and C. F. Roos, Nat. Phys. **8**, 277 (2012).
[7] T. Schaetz, C. R. Monroe, and T. Esslinger, New J. Phys. **15**, 085009 (2013).
[8] R. Blatt and D. Wineland, Nature (London) **453**, 1008 (2008).
[9] H. Haffner, C. Roos, and R. Blatt, Phys. Rep. **469**, 155 (2008).
[10] P. O. Schmidt, T. Rosenband, C. Langer, W. M. Itano, J. C. Bergquist, and D. J. Wineland, Science **309**, 749 (2005).
[11] D. J. Wineland, Rev. Mod. Phys. **85**, 1103 (2013).
[12] W. M. Itano, J. C. Bergquist, J. J. Bollinger, and D. Wineland, Phys. Scr. **T59**, 106 (1995).
[13] C. Monroe, D. M. Meekhof, B. E. King, S. R. Jefferts, W. M. Itano, D. J. Wineland, and P. Gould, Phys. Rev. Lett. **75**, 4011 (1995).
[14] B. Hemmerling, F. Gebert, Y. Wan, D. Nigg, I. V. Sherstov, and P. O. Schmidt, Appl. Phys. B **104**, 583 (2011).
[15] F. Gebert, Y. Wan, F. Wolf, J. C. Heip, and P. O. Schmidt, New J. Phys. **18**, 013037 (2016).
[16] S. C. Burd, D. T. C. Allcock, T. Leinonen, J. P. Penttinen, D. H. Slichter, R. Srinivas, A. C. Wilson, R. Jördens, M. Guina, D. Leibfried, and D. J. Wineland, Optica **3**, 1294 (2016).
[17] L. Deslauriers, P. C. Haljan, P. J. Lee, K.-A. Brickman, B. B. Blinov, M. J. Madsen, and C. Monroe, Phys. Rev. A **70**, 043408 (2004).
[18] J. F. Goodwin, G. Stutter, R. C. Thompson, and D. M. Segal, Phys. Rev. Lett. **116**, 143002 (2016).
[19] G. Santarelli, C. Audoin, A. Makdissi, P. Laurent, G. J. Dick, and A. Clairon, IEEE Trans. Ultrason. Ferroelectr. Freq. Control **45**, 887 (1998).
[20] Y. Wan, F. Gebert, F. Wolf, and P. O. Schmidt, Phys. Rev. A **91**, 043425 (2015).
[21] D. J. Wineland and W. M. Itano, Phys. Rev. A **20**, 1521 (1979).
[22] D. J. Wineland, C. Monroe, W. M. Itano, D. Leibfried, B. E. King, and D. M. Meekhof, J. Res. Natl. Inst. Stand. Technol. **103**, 259 (1998).
[23] Q. A. Turchette, C. J. Myatt, B. E. King, C. A. Sackett, D. Kielpinski, W. M. Itano, C. Monroe, and D. J. Wineland, Phys. Rev. A **62**, 053807 (2000).
[24] B. Hemmerling, Towards direct frequency comb spectroscopy using quantum logic, Ph.D. dissertation, Gottfried Wilhelm Leibniz Universität, Hannover, Germany, 2011, http://edok01.tib.uni-hannover.de/edoks/e01dh11/663868386.pdf.
[25] Q. A. Turchette, D. Kielpinski, B. E. King, D. Leibfried, D. M. Meekhof, C. J. Myatt, M. A. Rowe, C. A. Sackett, C. S. Wood, W. M. Itano, C. Monroe, and D. J. Wineland, Phys. Rev. A **61**, 063418 (2000).
[26] D. J. Wineland, W. M. Itano, J. C. Bergquist, and R. G. Hulet, Phys. Rev. A **36**, 2220 (1987).
[27] W. Paul, Rev. Mod. Phys. **62**, 531 (1990).
[28] K. Deng, H. Che, Y. Lan, Y. P. Ge, Z. T. Xu, W. H. Yuan, J. Zhang, and Z. H. Lu, J. Appl. Phys. **118**, 113106 (2015).
[29] K. Deng, Y. L. Sun, W. H. Yuan, Z. T. Xu, J. Zhang, Z. H. Lu, and J. Luo, Rev. Sci. Instrum. **85**, 104706 (2014). Other

instruments used are as follows: frequency synthesizer, Rohde-Schwarz SMB100A; RF amplifier, Minicircuits TIA-1000-1R8-2; Mg oven, Alvatec AS-3-Mg-100-V; photon-counting module, Hamamatsu H8259; electron-multiplying CCD, Andor EMCCD; and tunable diode laser system, Toptica FHG Pro.

[30] J. Zhang, W. H. Yuan, K. Deng, A. Deng, Z. T. Xu, C. B. Qin, Z. H. Lu, and J. Luo, Rev. Sci. Instrum. **84**, 123109 (2013).

[31] J.-S. Chen, S. M. Brewer, C. W. Chou, D. J. Wineland, D. R. Leibrandt, and D. B. Hume, Phys. Rev. Lett. **118**, 053002 (2017).